Conformal Ink-Jet Printed C-Band Phased-Array Antenna Incorporating Carbon Nanotube Field-Effect Transistor Based Reconfigurable True-Time Delay Lines

Maggie Yihong Chen, *Senior Member, IEEE*, Daniel Pham, *Member, IEEE*, Harish Subbaraman, *Member, IEEE*, Xuejun Lu, *Member, IEEE*, and Ray T. Chen, *Fellow, IEEE*

***Abstract*—We present a conformal ink-jet printed 2-bit four-element phased-array antenna (PAA) without any lithography process. Passive and active components, such as microstrip transmission lines, phase shifters, and RF power distribution networks are all developed adopting a room-temperature printing process. The PAA working at 5.2 GHz is printed on flexible DuPont Kapton flexible printed circuit polyimide film to demonstrate the conformal nature. High-speed carbon-nanotube-based field-effect transistors (FETs) function as switches to route the RF signal go through different segments of the true-time delay lines. The FET switch exhibits an ON–OFF ratio of over 1000 and current of 3.6 mA is obtained at a low source–drain bias of 0.8 V. The 2-bit azimuth beamsteering angles of the PAA are measured and confirmed to agree well with simulation values.**

***Index Terms*—Carbon nanotube (CNT), conformal antennas, field-effect transistor (FET) switches, ink-jet printing, phased-array antennas (PAAs).**

I. Introduction

PHASED-ARRAY antennas (PAAs) are more and more important in present-day communications since these antennas have low visibility, quick steering either electrically or optically controlled, and better directivity than do single antennas. Having so many advantages over the single antenna, PAAs are now widely used in both civilian operations, such as air traffic control and broadcast satellite communications, and in the military arena, such as marine radar, airborne radar, missile guidance, trajectory determination, and satellite communications.

Small size, lightweight, and low-power PAAs are attractive in accommodating the desired frequencies and data services in a restricted space. However, the PAA systems incorporate many components such as phase shifters, amplifiers, and feeding networks. Furthermore, the implementation of PAAs with monolithic microwave integrated circuits (MMICs) and RF microelectromechanical systems (MEMS) phase shifters requires high cost of packaging and integration of the system [1], [2]. One of the most recent studies in conformal phased-array antennas is the active membrane phased-array radar developing by the research group of the National Aeuronautics and Space Administration (NASA) Jet Propulsion Laboratory (JPL), Pasadena, CA [3]. However, the transmit/receive (T/R) module is assembled independently and attached to the membrane array, which greatly jeopardizes the reliability. Another recent advance in the development of lightweight flexible PAAs based on liquid crystal polymer (LCP) substrate was reported by the Georgia Institute of Technology, Atlanta [4]. However, this approach is dealing with the packaging issue, where the passive and active circuits are embedded in the multilayer 3-D system-on-a-package process. Low-profile conformal PAA designs would be ideal for simple integration into existing structures. However, such technology is still not totally mature. The major deterrent to such systems is the lack of high-speed electronic circuits fabricatable directly on a flexible surface [5], [6].

Current state-of-the-art flexible electronics are based on organic or polymer materials, such as regioregular poly (3-hexylthiophene) derivatives and pentacene. While the organic material based flexible electronic circuits can be monolithically integrated with flexible antennas, the carrier (electron or hole) mobility of these materials is less than 0.1 $\mathrm{cm}^2/\mathrm{V}\cdot\mathrm{s}$. Such low carrier mobility limits the operating frequency of the organic- or polymer-based flexible electronics circuit to a few kilohertz [7]. The low operating frequency makes this kind of electronics unsuitable for active PAA applications, where a multigigahertz operating frequency is required for different communication bands [8]–[12].

Individual carbon nanotube (CNT), a material with exceptional aspect ratio and great mechanical flexibility, was measured for extraordinary field-effect mobility as high as

Manuscript received August 08, 2011; accepted September 29, 2011. Date of publication November 10, 2011; date of current version December 30, 2011. This work was supported by the National Aeronautics and Space Administration (NASA) under Contract NNX08CB39P.

M. Y. Chen is with the Ingram School of Engineering, Texas State University, San Marcos, TX 78666 USA (e-mail: maggie.chen@txstate.edu).

D. Pham is with the Electrical and Computer Engineering Department, The University of Texas at Austin, Austin, TX 78758 USA (e-mail:thanhkhacpham@yahoo.com).

H. Subbaraman is with Omega Optics Inc., Austin, TX 78758 USA (e-mail: harish.subbaraman@omegaoptics.com).

X. Lu is with the Electrical and Computer Engineering Department, University of Massachusetts at Lowell, Lowell, MA 01854 USA (e-mail: xuejun_lu@uml.edu).

R. T. Chen is with the Electrical and Computer Engineering Department, The University of Texas at Austin, Austin, TX 78758 USA (e-mail: raychen@uts.cc.utexas.edu).

Color versions of one or more of the figures in this paper are available online at http://ieeexplore.ieee.org.

Digital Object Identifier 10.1109/TMTT.2011.2173209

0018-9480/$26.00 © 2011 IEEE

100 000 $cm^2/V \cdot s$ [13]. High field-effect mobility CNT thin-film transistors (CNT-TFTs) can be achieved by using ultrapure electronics-grade CNT solutions [14]. We printed CNT field-effect transistors (CNT-FETs) on a polyimide substrate with an ultrahigh operating frequency at 5 GHz [15] and applied it to construct a true-time delay feeding network to control a 2-bit two-element fully printed PAA [16]. We further purify the CNT material (more semiconducting) to eliminate the leakage current and increase the concentration of the CNT to increase the output current. The CNT-FET exhibits an ON–OFF ratio of over 1000 and current of 3.6 mA, compared to an ON–OFF ratio of 138 and current of 0.22 mA [15]. In this paper, we present the high-performance CNT-FET, as well as the fully ink-jet printed more complex 2-bit four-element PAA to demonstrate the scalability of the technology. Instead of traditional antenna manufacturing using copper etching techniques, flexible printed circuits (FPCs), or stamped antennas, we have developed room-temperature printable antennas using nanosilver particles solution. The feeding lines and power division are also printed using nano-silver particle solutions. The electronics, such as switch and amplifiers are printed with ultra-pure CNT solution without using any photolithography fabrication steps. A 2-bit four-element PAA working at 5.2 GHz is printed incorporating the FET switch-based true-time delay lines. Beamsteering of the PAA is demonstrated and compared with theoretical values.

II. Design of the 2-bit Four-Element PAA

A. Architecture Design of the 2-bit Four-Element PAA

For easy signal probing using a three-pin high-frequency RF probe, a coplanar waveguide is designed, as shown in Fig. 1(a). The big pads of signal and grounds are for the ease of probing. In order to make the most compact circuit, microstrip transmission lines are used to provide phase shifting. Therefore, after the RF signal is carried on the coplanar waveguide, a transition section is designed to convert coplanar waveguide to microstrip line. This structure can be analyzed as a six-port network with a ground plane, or three coupled microstrip lines [17]. The designed pattern of the transition is in the middle part of Fig. 1(b). The coupling region is chosen to be $L = \lambda_g/4$, where λ_g is the guided wavelength of the three-conductor line [18].

Fig. 2 shows the architecture of the 2-bit true-time delay feeding network for a four-element PAA. First, the RF signal is split into four branches, with each branch split again by a 1×2 power splitter. Through programming, the status of each pair of FET switchs (such as pair "1" and "3", pair "2" and "4"), the signal experiences different time delay. Consequently, different steering angles can be achieved. The time delay between adjacent elements of a PAA can be calculated as

$$t = \frac{d\sin(\theta)}{c} \tag{1}$$

where d is the distance between adjacent element, c is the light velocity, and θ is the beam-steering angle. In our design, d is less than a half-wavelength to avoid the grating effect. The length difference between delay lines can be calculated as

$$L_{\text{diff}} = \frac{t * c}{n} \tag{2}$$

where n is the refractive index of the microwave propagation media.

Four possible azimuth steering angles are designed according to the above equations, which are $-24°$, $0°$, $24°$, and $54°$.

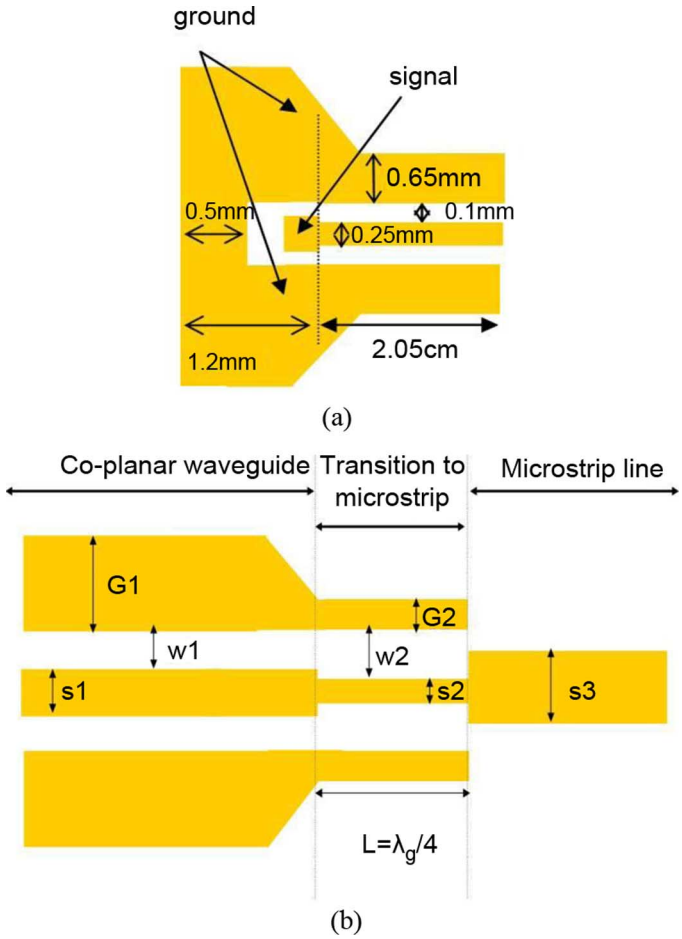

Fig. 1. (a) Designed pattern of coplanar-waveguide probing. (b) Coplanar waveguide to microstrip line transition.

B. Design of High-Speed FET

Fig. 3 is a schematic diagram showing the structure of the CNT-FET. To begin with, there is a substrate that exists on the bottom layer, where the substrate that may be used in the present invention includes, but is not limited to paper, polyethylene terephtalate (PET), FR4, Kapton, indium tin oxide (ITO) glass, metal foils, fabrics, and silicon wafer. The source and drain electrodes of the transistor are printed on top of the substrate, with thickness varying from hundreds of nanometers to a few micrometers depending on the material, printer nozzle size, and resolution. The conductive electrode materials include, but are not limited to conductive silver fluids, conductive copper fluids, and conductive polymer. The CNT layer is then printed on top of the electrode layer. Multiple layers of CNT are printed to reduce the resistance and to build a strong CNT network. The

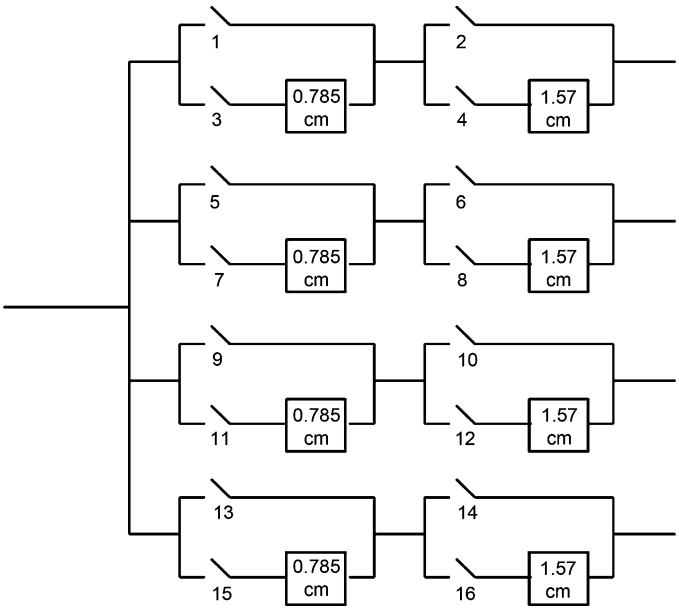

Fig. 2. Architecture of the 2-bit true-time delay feeding network for a four-element phased-array antenna.

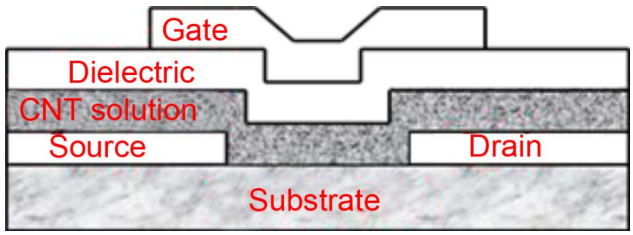

Fig. 3. Schematic structure of the CNT-based FET.

CNT layer serves as the channel layer. Next, the isolation dielectric layer is printed on top of the CNT layer. The isolation layer is used to isolate the gate from the channel CNT layer, source, and drain. At last, the gate electrode is printed on top of the isolation layer. The gate voltage is used to control the resistance of the CNT channel layer between the source and drain. A slight change in the gate voltage can make dramatic changes in the conductivity of the channel layer.

III. Fabrication and Measurement of the PAA

The entire 2-bit four-element PAA is printed using the Fujifilm Dimatix DMP-2831 materials deposition system on a DuPont Kapton FPC polyimide film [19], which is used in a wide variety of applications such as substrates for FPCs, transformer and capacitor insulation, and bar-code labels. The fabrication procedure of the 2-bit four-element PAA is illustrated in Fig. 4. First, the coplanar input coupler, power splitter, and transmission lines are printed together with the source and drain electrodes of FETs on the Kapton FPC polyimide film using the silver nanoparticle ink from Cabot, Albuquerque, NM, followed by the thermal annealing at 130 °C for 30 min. Multiple printing is carried out to increase the thickness of source and drain. The separation between the source and drain electrodes, i.e., channel length, is 100 μm and the width of the channel is 300 μm. From recent publication [20], depending on the length of the CNT, the device channel length has to be

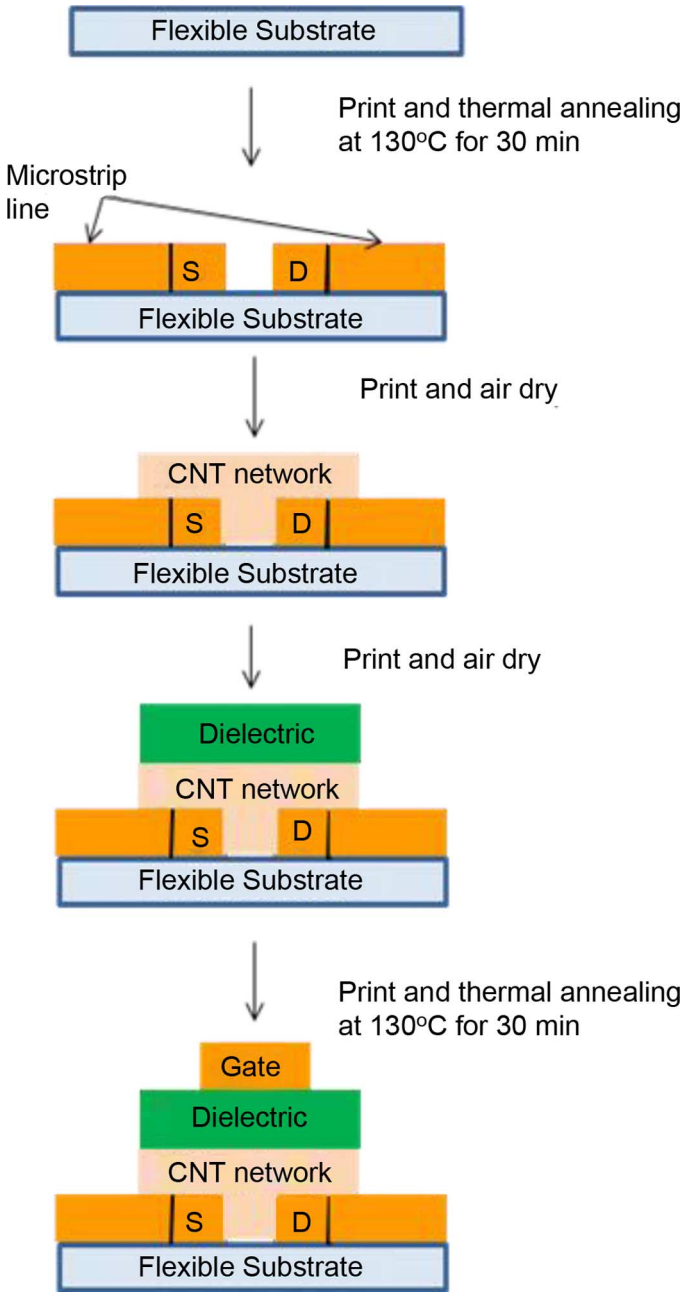

Fig. 4. Fabrication procedure of the 2-bit four-element PAA.

much longer than the CNT length (more than ten times) to avoid OFF stage leakage due to the metallic CNT. Therefore, we deposited a channel length of 100 μm to further reduce the possibility of the leakage from some left metallic CNTs. An active carrier transport layer is then printed using an ultrapure electronics-grade CNT solution. After printing, the active layer is left at room temperature in the open air to dry. A thin layer of dielectric is then printed on top of the CNT film as the gate dielectric. In the last step, a silver nanoparticle ink layer is printed as the top gate electrode. Fig. 5 shows a microscope image of the fabricated FET and delay lines.

A. Characterization and Analysis of High-Speed FET

Fig. 6 shows the source–drain I–V characteristics (I_{DS} versus V_{DS}) of the CNT-FET at different gate voltages (V_G). The gate

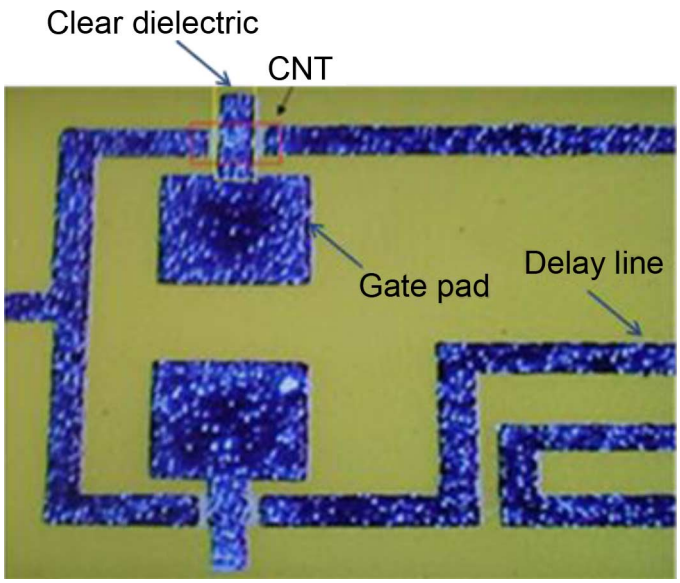

Fig. 5. Microscope image of the fabricated FET and delay lines.

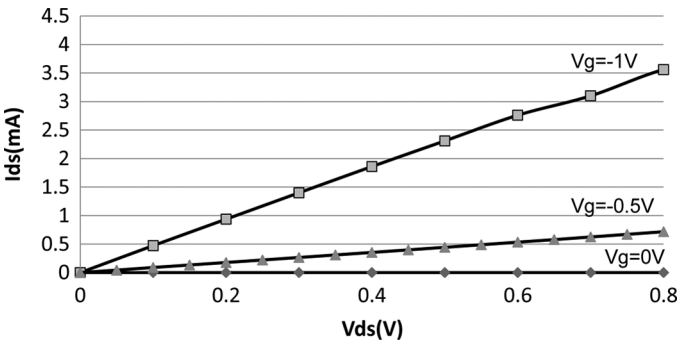

Fig. 6. *I–V* curve of a fabricated flexible FET.

voltages vary from −1 to 0 V. At the same source–drain voltage $(V_{\rm DS})$, lower source–drain currents $(I_{\rm DS})$ are observed as the gate voltage increases from negative to zero voltages. This indicates that the CNT network in this FET is a p-type carrier (hole) transport layer. At the source–drain voltage $(V_{\rm DS})$ of 0.8 V, a high source–drain current $(I_{\rm DS})$ of 3.6 mA and a low $I_{\rm DS}$ of 3.4 μA are obtained at the gate voltage of −1.0 and 0 V, respectively. The source–drain current $(I_{\rm DS})$ ON–OFF ratio is over 1000. The large ON–OFF ratio reveals a high content of the semiconducting type of CNTs in the CNT active layer. The gate–source leakage current $(I_{\rm GS})$ is measured to be in the pA range. The high-speed modulation performance of the CNT switch with 50-Ω transmission line was tested and published in [15], with the equivalent circuit shown there.

B. Characterization of 2-bit Four-Element PAA

A photograph of the printed 2-bit four-element PAA subsystem using the proposed material and method with a DMP-2831 materials deposition system is shown in Fig. 7. Each patch antenna element has the size of 24.1 mm × 20.5 mm. The distance between adjacent elements is less than a half-wavelength to avoid grating lobes. The entire array, including the feed and phase shifters, has the size of 111.4 mm × 52.1 mm.

First, the RF signal from the vector network analyzer is applied on the coplanar waveguide using the microwave probe

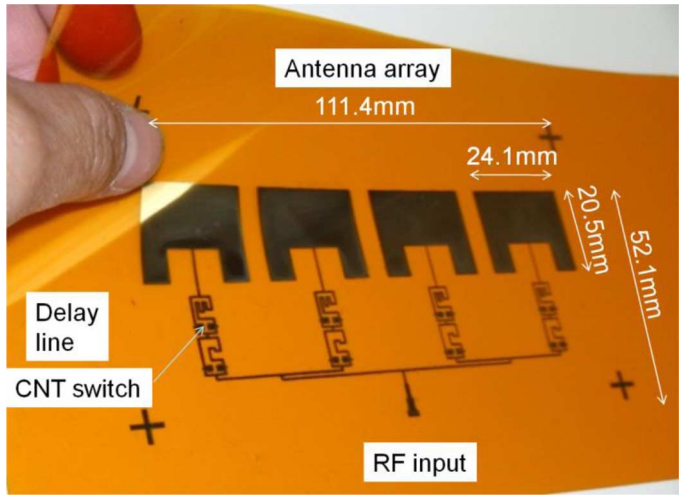

Fig. 7. Photograph of the printed 2-bit four-element PAA.

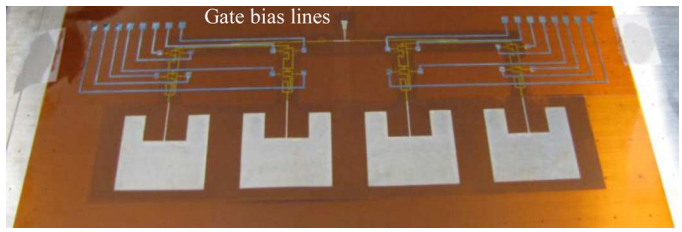

Fig. 8. Photograph of the two-layer 2-bit four-element PAA with metal gate bias lines.

with working frequency up to 50 GHz. The signal on the coplanar waveguide is then transitioned onto microstrip transmission line through the transition section based on a three-line coupler. The signal is then split into two branches, with each branch split again by a 1 × 2 splitter. The signals through the four paths experience different phase shifts due to different lengths of delay lines. FET switches select appropriate signals from the delay lines to feed the antenna elements. By appropriately programming the on/off status of the 16 FET switches, the four-element antenna array is steered accordingly.

Two-layer metal interconnect is also developed to provide connection to the gate electrodes from an external power supply. A thin Kapton (25 μm) substrate with adhesive coating on one side is bonded on top of the first substrate containing the printed PAA subsystem shown in Fig. 7. Contact vias are formed prior to attaching in order to obtain metal contacts with the gate contact pads on the first substrate. A pressurized annealing process at 100 °C is used to bond these layers together. Silver ink is then printed on the top layer to form the metal gate bias lines. Fig. 8 shows a photograph of the two-layer fully fabricated 2-bit four-element PAA system.

The 8510C HP network analyzer provides RF output power of 9.9 dBm to the flexible PAA through the RF probe. A 16-dBi standard gain horn is used as the receiving antenna, with the receiving power measured by a microwave spectrum analyzer (MSA). The gain of the antenna array is measured to be 10.25 dBi and the efficiency is calculated to be 42%, including the loss of transmission line, FET switch, and coupling loss of RF probes.

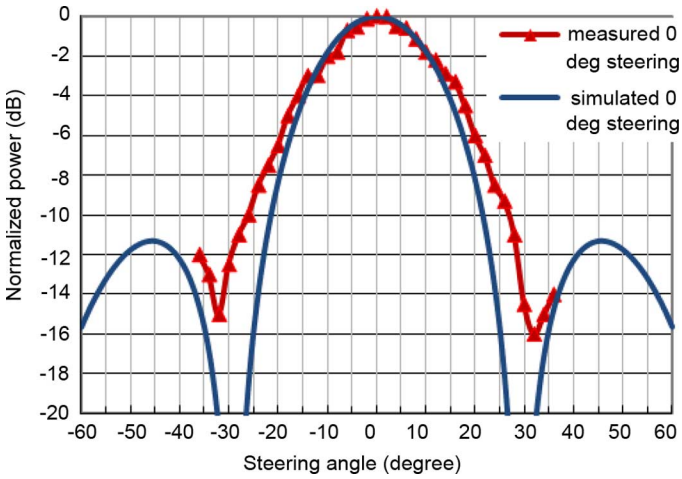

Fig. 9. Theoretical values and measurement results of far field patterns for 0° steering.

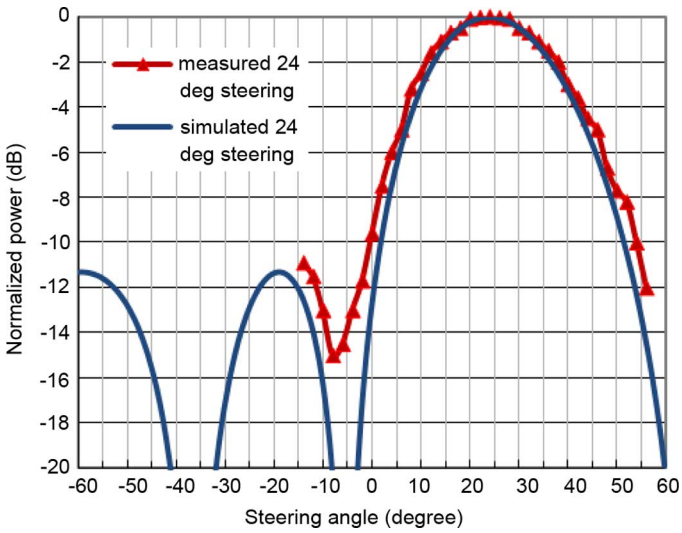

Fig. 10. Theoretical values and measurement results of far field patterns for 24° steering.

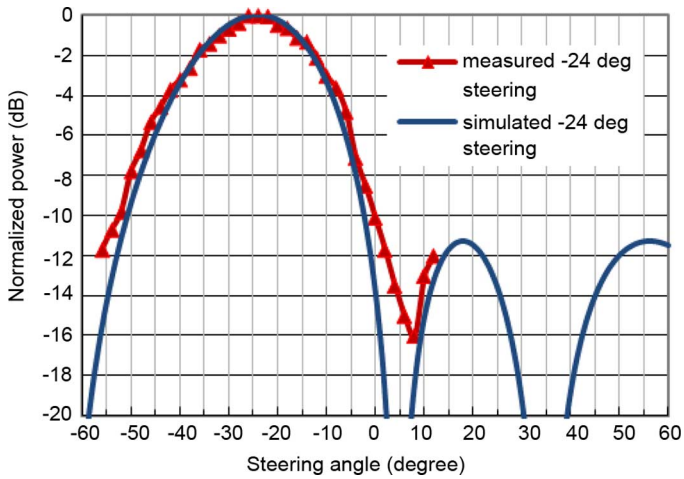

Fig. 11. Theoretical values and measurement results of far-field patterns for $-24°$ steering.

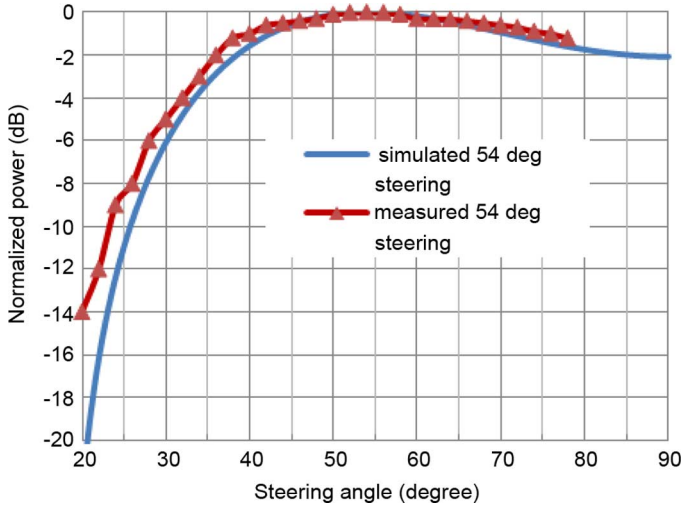

Fig. 12. Theoretical values and measurement results of far-field patterns for 54° steering.

In order to estimate the insertion loss of the CNT switch, we short circuit the S and D of the CNT switch numbering 1, 2, 5, 6, 9, 10, 13, and 14 by a microstrip line for 0° steering. The gain of the antenna array is measured to be 12.12 dBi. Compared with 10.25 dBi with CNT switches, the insertion loss of each switch is estimated to be 0.23 dB.

The signal strength at various angles is measured to get the far-field patterns. We measure all four azimuth steering angles. At 0° steering, switches numbering 1, 2, 5, 6, 9, 10, 13, and 14 are closed. Switch numbering 3, 4, 7, 8, 11, 12, 15, and 16 are open. The switches are biased with $V_{\rm DS} = 0.8$ V and $V_G = 0$ or -1 V for the open or closed states, respectively. Each closed switch has a dc current of 3.5 mA, and the array consumes a total dc power of 22.4 mW. The four delay lines feed the delayed signal to the four antenna elements. $S11$ is measured to be -18.1 dB. The far-field pattern with theoretical values and measurement results are compared in Fig. 9. The beamwidth is measured to be 28°.

At 24° steering, switches numbering 1, 2, 6, 7, 9, 12, 15, and 16 are closed. Switch numbering 3, 4, 5, 8, 10, 11, 13, and 14 are open. The four delay lines feed the delayed signal to the four antenna elements. $S11$ is measured to be -17.6 dB. The far-field pattern with theoretical values and measurement results are compared in Fig. 10. The beamwidth is measured to be 31°.

At $-24°$ steering, switches numbering 3, 4, 5, 8, 10, 11, 13, and 14 are closed. Switches numbering 1, 2, 6, 7, 9, 12, 15, and 16 are open. The four delay lines feed the delayed signal to the four antenna elements. $S11$ is measured to be -17.7 dB. The far-field pattern with theoretical values and measurement results are compared in Fig. 11. The beamwidth is measured to be 30°.

At 54° steering, only the top two delay lines can be utilized to provide delay for two antenna elements. Switches numbering 1, 2, 7, and 8 are closed, and all the others are open. $S11$ is measured to be -18.5 dB. The far-field pattern with theoretical values and measurement results are compared in Fig. 12.

IV. Conclusion

In summary, we have demonstrated an all-ink-jet-printed conformal 2-bit four-element active PAA operating at 5.2 GHz on a DuPont Kapton FPC polyimide film by using a DMP-2831 materials deposition system. The true-time delay lines incorporated the high-speed CNT-based FET switches are proven to work well through the beamsteering experiments of the PAA.

All the fabrication processes are performed at room temperature. Such a low-temperature processing method allows us to use virtually any kind of a flexible substrate such as a regular slide transparency for fabrication, as demonstrated in our study. By incorporating all passive and active components, including phase shifters, power splitters, amplifiers, and antennas, a fully functioned PAA can be printed at low cost and fast production. The system can be easily repaired by reprint failed devices. This technology can be readily applied to RF identification (RFID), sensor, smart skin, and electronic paper areas.

The measured beam-steering angles agree well with simulation and serve as the confirmation of the printed flexible PAA.

ACKNOWLEDGMENT

The authors would like to thank Dr. F. A. Miranda, Dr. A. Zaman, and J. Nessel, all with the NASA Glenn Research Center, Cleveland, OH, for helpful discussions.

REFERENCES

[1] L. Whicker, "Active phased array technology using coplanar packaging technology," *Trans. Antennas Propag.*, vol. 43, no. 9, pp. 949–952, Sep. 1995.

[2] Y. Mancuso, P. Gremillet, and P. Lacomme, "T/R-modules MTT-S technological and technical trends for phased array antennas," in *IEEE MTT-S Int. Microw. Symp. Dig.*, Jun. 2006, pp. 614–617.

[3] A. Moussessian, L. D. Castillo, J. Huang, G. Sadowy, J. Hoffman, P. Smith, T. Hatake, C. Derksen, B. Lopez, and E. Caro, "An active membrane phased array radar," in *IEEE MTT-S Int. Microw. Symp. Dig.*, Long Beach, CA, Jun. 2005, pp. 1711–1714.

[4] D. J. Chung, S. Bhattacharya, G. Ponchak, and J. Papapolymerou, "Recent advances in the development of a lightweight, flexible 16×16 antenna array with RF MEMS shifters at 14 GHz," in *8th Annu. NASA Earth Sci. Technol. Conf.*, Jun. 2008.

[5] J. J. Komiak *et al.*, "Design and performance of octave S/C-band MMIC T/R modules for multi-function phased arrays," *IEEE Trans. Microw. Theory Tech.*, vol. 39, no. 12, pp. 1955–1963, Dec. 1991.

[6] T. Sasaki *et al.*, "Ultra small size X band MMIC T/R module for active phased array," in *IEEE MTT-S Int. Microw. Symp. Dig.*, 1992, pp. 1531–1534.

[7] H. Meiling and R. E. I. Schropp, "Stable amorphous-silicon thin-film transistors," *Appl. Phys. Lett.*, vol. 70, pp. 2681–2683, 1997.

[8] S. Jeon, Y.-W. Kim, and D.-G. Oh, "A new active phased array antenna for mobile direct broadcasting satellite reception," *IEEE Trans. Broadcast.*, vol. 46, no. 1, pp. 34–40, Mar. 2000.

[9] R. A. Flynt, F. Lu, J. A. Navarro, and C. Kai, "Low cost and compact active integrated antenna transceiver for system applications," *IEEE Trans. Microw. Theory Tech.*, vol. 44, no. 10, pp. 1642–1649, Oct. 1996.

[10] A. Dreher, N. Niklasch, F. Klefenz, and A. Schroth, "Antenna and receiver system with digital beamforming for satellite navigation and communications," *IEEE Trans. Microw. Theory Tech.*, vol. 51, no. 7, pp. 1815–1821, Jul. 2003.

[11] Huang, Lou, Feria, and Kim, "An inflatable L-band microstrip SAR array," in *IEEE AP-S/URSI Symp.*, Atlanta, GA, Jun. 1998, pp. 2100–2103.

[12] J. Huang and A. Moussessian, "Thin-membrane aperture coupled L-band patch antenna," in *IEEE AP-S/URSI Symp.*, Monterey, CA, Jun. 2004, pp. 2388–2391.

[13] T. Durkop, S. A. Getty, E. Cobas, and M. S. Fuhrer, "Extraordinary mobility in semiconducting carbon nanotubes," *Nano Lett.*, vol. 4, pp. 35–39, 2004.

[14] P. Nikolaev, M. J. Bronikowski, R. K. Bradley, F. Rohmund, D. T. Colbert, K. A. Smith, and R. E. Smalley, "Gas-phase catalytic growth of single-walled carbon nanotubes from carbon monoxide," *Chem. Phys. Lett.*, vol. 313, pp. 91–97, 1999.

[15] J. Vaillancourt, H. Zhang, P. Vasinajindakaw, H. Xia, X. Lu, X. Han, D. C. Janzen, W.-S. Shih, C. S. Jones, M. Stroder, M. Y. Chen, H. Subbaraman, R. T. Chen, U. Berger, and M. Renn, "All ink-jet printed carbon nanotube (CNT) thin-film transistor on a polyimade substrate with an ultrahigh operating frequency of over 5 GHz," *Appl. Phys. Lett.*, vol. 93, 2008, Art. ID 243301.

[16] M. Y. Chen, X. Lu, H. Subbaraman, and R. T. Chen, "Fully printed phased-array antenna for space communications," in *SPIE Defense, Security, Sens. Conf.*, 2009, pp. 731814-1–731814-6.

[17] D. Pavlidis and H. L. Hartnagel, "The design and performance of three-line microstrip couplers," *IEEE Trans. Microw. Theory Tech.*, vol. MTT-24, no. 10, pp. 631–640, Oct. 1976.

[18] P. G. Gauthier *et al.*, "W-band finite ground coplanar waveguide (FGCPW) to microstrip line transition," in *IEEE MTT-S Int. Microw. Symp. Dig.*, 1998, pp. 107–109, Art. ID TU2E-3.

[19] DuPont, Circleville, OH, "DuPont Kapton polyimide film," DuPont Kapton Product Data Sheet, YEAR. [Online]. Available: http://www2.dupont.com/Kapton/en_US/assets/downloads/pdf/FPC_datasheet.pdf

[20] N. Pimparkar, Q. Cao, J. A. Rogers, and M. A. Alam, "Theory and practice of striping for improved ON/OFF ratio in carbon nanonet thin film transistors," *Nano Res.*, vol. 2, pp. 167–175, 2009.

Maggie Yihong Chen (M'03–SM'08) received the B.S. and M.E. degrees in electrical engineering and Ph.D. degree in electrical engineering from The University of Texas at Austin, in 1993, 1996, and 2002, respectively.

She is currently an Assistant Professor with Texas State University (TSU), San Marcos. Prior to joining TSU, she was a Senior Scientist with Omega Optics Inc., Austin TX. She has authored or coauthored over 60 publications in refereed journals and conferences. Her research over the past ten years has been focused on nanoelectronics, optical true-time delay beamforming for PAAs, and nanophotonics.

Dr. Chen is a Senior Member of the Optical Society of America (OSA) and the International Society for Optics and Photonics (SPIE). She was the conference chair of the International Conferences on Optoelectronic Devices and Integration, Photonics Asia, in 2004 and 2007.

Daniel Pham (A'01–M'01) received the B.S degree in chemical engineering from Texas A&M University, College Station, the M.S. degree in chemical engineering from Rice University, Houston, TX, and the Ph.D. degree in electrical and computer engineering from The University of Texas at Austin, in 2010.

He worked in the semiconductor industry for over ten years, during which time he was focused on semiconductor processes, device integration, and novel device research. He has authored or coauthored over 25 publications. He holds eight patents.

Harish Subbaraman (M'11) received the B.E. degree in electronics and communication engineering from the Chaitanya Bharathi Institute of Technology, Hyderabad, India, in 2004, and the M.S. and Ph.D. degrees in electrical engineering from The University of Texas at Austin, in 2006 and 2009, respectively.

He has authored or coauthored over 15 publications in refereed journals and conferences.

Xuejun Lu (M'02) photograph and biography not available at time of publication.

Ray T. Chen, (M'91–SM'98–F'04), photograph and biography not available at time of publication.